

Like a rolling stone: colonization and migration dynamics of the grey reef shark (*Carcharhinus amblyrhynchos*)

Pierre Lesturgie¹, Camrin Braun², Eric Clua³, Jeremy Kiszka⁴, Johann Mourier⁵, Simon Thorrold², Thomas Vignaud⁶, Serge Planes³, and Stefano Mona¹

¹Institut de Systématique Evolution Biodiversité

²Woods Hole Oceanographic Institution

³EPHE PSL

⁴FIU

⁵Université de Corse Pasquale Paoli

⁶CRIOBE

October 7, 2022

Abstract

Designing appropriate management plans requires knowledge of both the dispersal ability and what has shaped the current distribution of the species under consideration. Here we investigated the evolutionary history of the endangered grey reef shark (*Carcharhinus amblyrhynchos*) across its range by sequencing thousands of RAD-seq loci in 173 individuals in the Indo-Pacific (IP). We first bring evidence of the occurrence of a range expansion (RE) originating close to the Indo-Australian Archipelago (IAA) where two stepping-stone waves (east and westward) colonized almost the entire IP. Coalescent modeling additionally highlighted a homogenous connectivity ($Nm \sim 10$ per generation) throughout the range, and an isolation by distance model suggested the absence of barriers to dispersal despite the affinity of *C. amblyrhynchos* to coral reefs. This coincides with long-distance swims previously recorded, suggesting that the strong genetic structure at the IP scale ($F_{ST} \sim 0.56$ between its ends) is the consequence of its broad current distribution and organization in a large number of demes. Our results strongly suggest that management plans for the grey reef shark should be designed on a range-wide rather than a local scale due to its continuous genetic structure. We further contrasted these results with those obtained previously for the sympatric but strictly lagoon-associated *Carcharhinus melanopterus*, known for its restricted dispersal ability. *C. melanopterus* exhibits similar RE dynamic, but is characterized by stronger genetic structure and a non-homogeneous connectivity largely dependent on local coral reefs availability. This sheds new light on shark evolution, emphasizing the roles of IAA as source of biodiversity and of life history traits in shaping the extent of genetic structure and diversity.

1 **Like a rolling stone: colonization and migration dynamics of the grey**
2 **reef shark (*Carcharhinus amblyrhynchos*)**

3

4 Running title: Evolutionary history of the grey reef shark.

5

6 Pierre Lesturgie¹, Camrin D. Braun², Eric Clua^{3,4}, Jeremy Kiszka⁵, Johann Mourier^{3,6}, Simon R.
7 Thorrold², Thomas Vignaud³, Serge Planes^{3,4}, Stefano Mona^{1,3,*}

8

9 ¹ Institut de Systématique, Evolution, Biodiversité, ISYEB (UMR 7205), Muséum National
10 d'Histoire Naturelle, CNRS, Sorbonne Université, EPHE, Université des Antilles, Paris, France.

11 ² Biology Department, Woods Hole Oceanographic Institution, Woods Hole, MA 02543, USA

12 ³ Laboratoire d'Excellence CORAIL, Papetoai, French Polynesia.

13 ⁴ PSL Research University: EPHE-UPVD-CNRS, USR 3278 CRIOBE, Université de Perpignan,
14 52 Avenue Paul Alduy, 66860, Perpignan, Cedex, France

15 ⁵ Institute of Environment, Department of Biological Sciences, Florida International University,
16 North Miami, USA

17 ⁶ Université de Corse Pasquale Paoli, UMS 3514 Plateforme Marine Stella Mare, 20620
18 Biguglia, France

19

20 * Author for corresponding: Stefano Mona Institut de Systématique, Evolution, Biodiversité,
21 ISYEB (UMR 7205), Muséum National d'Histoire Naturelle, CNRS, Sorbonne Université,
22 EPHE, Université des Antilles, Paris, France, stefano.mona@mnhn.fr.

23

24

Abstract

25

26

27

28

29

30

31

32

33

34

35

36

37

38

39

40

41

42

43

44

45

46

Designing appropriate management plans requires knowledge of both the dispersal ability and what has shaped the current distribution of the species under consideration. Here we investigated the evolutionary history of the endangered grey reef shark (*Carcharhinus amblyrhynchos*) across its range by sequencing thousands of RAD-seq loci in 173 individuals in the Indo-Pacific (IP) . We first bring evidence of the occurrence of a range expansion (RE) originating close to the Indo-Australian Archipelago (IAA) where two stepping-stone waves (east and westward) colonized almost the entire IP. Coalescent modeling additionally highlighted a homogenous connectivity ($Nm \sim 10$ per generation) throughout the range, and an isolation by distance model suggested the absence of barriers to dispersal despite the affinity of *C. amblyrhynchos* to coral reefs. This coincides with long-distance swims previously recorded, suggesting that the strong genetic structure at the IP scale ($F_{ST} \sim 0.56$ between its ends) is the consequence of its broad current distribution and organization in a large number of demes. Our results strongly suggest that management plans for the grey reef shark should be designed on a range-wide rather than a local scale due to its continuous genetic structure. We further contrasted these results with those obtained previously for the sympatric but strictly lagoon-associated *Carcharhinus melanopterus*, known for its restricted dispersal ability. *C. melanopterus* exhibits similar RE dynamic, but is characterized by stronger genetic structure and a non-homogeneous connectivity largely dependent on local coral reefs availability. This sheds new light on shark evolution, emphasizing the roles of IAA as source of biodiversity and of life history traits in shaping the extent of genetic structure and diversity.

Keywords: Meta-population, Rad-seq, demographic history, range expansion, *Carcharhinus amblyrhynchos*, *Carcharhinus melanopterus*.

47

Introduction

48 More than 37% of shark species are currently threatened with extinction (Dulvy et al., 2021) and
49 less than 30% are on stable or increasing population trend according to the International Union for
50 Conservation of Nature (IUCN) Red List of threatened species. As meso or apex predators, they
51 hold important roles in their ecosystems (Bornatowski, Navia, Braga, Abilhoa, & Corrêa, 2014)
52 and their decline has already shown negative cascading effects on food web structure (Friedlander
53 & DeMartini, 2002; Myers, Baum, Shepherd, Powers, & Peterson, 2007). Although local-scale
54 conservation programs have been established, their efficiency has been questioned for some
55 species of sharks (Robbins, Hisano, Connolly, & Choat, 2006; Speed et al., 2016). For instance,
56 local-scale management might not always be consistent with the home range size and the dispersal
57 ability of sharks (but see Dwyer et al. (2020)). Genetics and ecological evidence have identified
58 both species with very restricted home ranges (Mourier, Mills, & Planes, 2013; Whitney, Robbins,
59 Schultz, Bowen, & Holland, 2012) and species capable of crossing large expanses of ocean
60 (Bailleul et al., 2018; Corrigan et al., 2018; Pirog et al., 2019). Designing appropriate management
61 actions is therefore a difficult task requiring the knowledge of both the dispersal ability of the
62 species under investigation and the existence of barriers to gene flow, which are often hard to
63 identify in the marine realm.

64 Population genomics is becoming increasingly important in this context, particularly because of
65 the large amount of data provided by the emergence of next generation sequencing approaches
66 (NGS). It is now possible to assess the genetic diversity of model or non-model species at an
67 unprecedented level of accuracy (Benazzo et al., 2017; Steiner, Putnam, Hoeck, & Ryder, 2013).
68 However, genetic diversity alone does not provide clues on the evolutionary trajectory of a species
69 and a careful modelling is required to fully understand its demographic history as well as the

70 conservation challenges to be faced. Unfortunately, for computational reasons, many commonly
71 used software implement, under different algorithms, *unstructured* models, i.e., models that
72 consider the population under investigation as isolated or panmictic (Heled & Drummond, 2008;
73 Heller, Chikhi, & Siegismund, 2013; Li & Durbin, 2011; Liu & Fu, 2015). Except for highly vagile
74 species which are panmictic at a large scale (Corrigan et al., 2018; Lesturgie, Planes, & Mona,
75 2022; Pirog et al., 2019), broadly distributed sharks species are more likely organized in meta-
76 population(s) throughout their range (Maisano Delser et al., 2019, 2016; Momigliano et al., 2017;
77 Pazmiño et al., 2018). The application of *unstructured* models to species organised in meta-
78 populations yield spurious signatures of effective populations size (N_e) changes through time
79 (Chikhi, Sousa, Luisi, Goossens, & Beaumont, 2010; Maisano Delser et al., 2019; Mazet,
80 Rodríguez, Grusea, Boitard, & Chikhi, 2016; Mazet, Rodríguez, & Chikhi, 2015), with potentially
81 dangerous consequences in terms of conservation policies. However, recent studies have
82 highlighted the usefulness of such models to characterize the gene genealogy of the sampled
83 lineages which in turn reveals important features of the meta-population (Arredondo et al., 2021;
84 Lesturgie et al., 2022; Rodríguez et al., 2018). This emphasizes the necessity to couple complex
85 meta-population models and *unstructured* models when uncovering the demographic history of a
86 species.

87 Here we investigated the evolutionary history of the grey reef shark *Carcharhinus amblyrhynchos*,
88 a coral reef-associated shark inhabiting the tropical Indo-Pacific. While *C. amblyrhynchos* is
89 considered one of the most abundant reef sharks in the Indo-Pacific, it is listed as Endangered on
90 the IUCN red list of threatened species. With a mean size of ~190 cm (Compagno, 2001), *C.*
91 *amblyrhynchos* inhabits either fringing or barrier reefs and displays patterns of reef fidelity
92 (Barnett, Abrantes, Seymour, & Fitzpatrick, 2012; Espinoza, Heupel, Tobin, & Simpfendorfer,

93 2014) as well as philopatry (Field, Meekan, Speed, White, & Bradshaw, 2011). Tagging studies
94 have indicated long range movement up to ~900 km (Barnett et al., 2012; Bonnin et al., 2019),
95 which raise questions about the extent of residency patterns for this species. Previous molecular
96 studies using both microsatellites and Rad-sequencing did not find signatures of genetic structure
97 at a low geographic scale such as the Great Barrier Reef (Momigliano et al., 2017; Momigliano,
98 Harcourt, Robbins, & Stow, 2015) and the Phoenix Islands archipelago (Boissin et al., 2019).
99 Conversely, isolation by distance patterns have been found at larger scale and some evidence
100 suggests that coastal abundance of reef can fuel genetic exchanges, while oceanic expanses are
101 barriers to gene flow (Boissin et al., 2019; Momigliano et al., 2017).

102 To shed light on these contrasting findings, we sequenced DNA from 203 individuals of *C.*
103 *amblyrhynchos* sampled at 18 sites covering most of its distribution range (Figure 1) following a
104 double digest restriction site associated DNA protocol (dd-RADseq, Peterson et al. 2012). The
105 large panel of assembled loci was used to: (i) detect the occurrence and origin location of a range
106 expansion (RE); (ii) investigate its demographic history by implementing both meta-population
107 and *unstructured* models; (iii) reassess the population structure of the grey reef shark in the Indo-
108 Pacific. We finally compared the results here obtained with those previously found in the blacktip
109 reef shark (*Carcharhinus melanopterus* (Maisano Delser et al., 2019, 2016)). The two species
110 share a very similar distribution in the Indo-Pacific but are characterized by different habitat
111 preferences and life-history traits, providing an excellent opportunity to improve our knowledge
112 on the biology of sharks.

113

114 Material and Methods

115 Sampling and Rad sequencing

116 We collected 203 samples of *C. amblyrhynchos* that covered most of its longitudinal distribution
117 range (Figure 1), with two sampling sites in the Mozambique Channel in the western Indian Ocean
118 (IND – Juan de Nova and Zélée bank) and 16 in the Pacific Ocean (PAC). Among the PAC
119 sampling sites, four were chosen in the Coral Sea (COR): two in the Chesterfield Islands (Bampton
120 and Avond) and two in New Caledonia (Belep and Poindimie). The remaining samples came from
121 the Central and Easter Pacific (CPA): six in the Phoenix Islands (Enderbury, Kanton, McKean,
122 Niku, Orona and Birnie) one in Palmyra Island and five in French Polynesia (Fakarava, Moorea,
123 Faaite, Raraga and Nengo) (Figure 1, Table 1). Total genomic DNA has been extracted and
124 conserved in 96% ethanol using QIAGEN DNeasy Blood and Tissue purification kit (Qiagen,
125 Hilden, Germany) according to the manufacturer's protocols. We followed the double digest
126 restriction site associated DNA (dd-RADseq) protocol of (Peterson et al., 2012) to create a
127 genomic library, using EcoRI and MSFI as restriction enzymes. We selected fragments of ~400
128 bp length and sequenced with Illumina HiSeq 2500 machine (single-end, 125 bp).

129 In the absence of a reference genome, we assembled loci *de novo* using *Stacks* v.2.5 (Rochette,
130 Rivera-Colón, & Catchen, 2019). Briefly, we demultiplexed the reads through the
131 *process_radtags.pl* script and assembled the loci using the *denovo_map.pl* pipeline with the
132 parameters $m=3$ (minimum read depth to create a stack), $M=3$ (number of mismatches allowed
133 between loci within individuals) and $n=3$ (number of mismatches allowed between loci within
134 catalogue). We found a mean depth of coverage (over individuals and loci) of ~10x (see Results).
135 Previous work suggested that such low-coverage value may bias a correct genotype calling under
136 the algorithm implemented in *Stacks* v.1, *Stacks* v.2 and *PyRAD* by skewing the site frequency

137 spectrum (SFS) towards an excess of low frequency variants (Mona et al. in prep; see
138 supplementary materials for details). For this reason, we followed two different bioinformatics
139 pipelines: the first to obtain a dataset to perform analyses based on the SFS (genetic diversity,
140 range expansion and historical demographic inferences) and the second to investigate population
141 structure, for which low frequency variants are not informative and are removed before the
142 downstream analyses.

143

144 Genetic diversity

145 We followed the genotype free estimation of allele frequencies pipeline implemented in the
146 software *ANGSD* v.0.923 (Korneliussen, Albrechtsen, & Nielsen, 2014). This approach has been
147 suggested to be more efficient for low to medium coverage NGS data than SNPs calling algorithms
148 (Korneliussen et al., 2014). *ANGSD* requires a reference sequence to work. To this end, we
149 followed the framework proposed by Khimoun et al. (2020) and Heller et al. (2021) which we
150 applied to each sampling site separately to maximise the number of loci: i) we assembled Rad loci
151 present in at least 80% of the sampled individuals using *Stacks* with the same parameters as above
152 (i.e., $m=M=n=3$); ii) we concatenated the consensus sequences for each locus, to which we added
153 a stretch of 120 “N” in order to facilitate mapping, to create an artificial reference sequence; iii)
154 we mapped raw reads from individual *fastq* files using the *bwa-mem* algorithm with default
155 parameters (Li & Durbin, 2009) against the artificial reference sequence. Using *ANGSD* filters, we
156 discarded (1) sites with a coverage < 3 (using the flag *-minIndDepth 3*) (2) poor quality and mis-
157 aligned reads (with default parameters and flags *-minQ20* and *-minMapQ 20*), (3) poor quality
158 bases (with default parameters and flags *-baq 1* and *-C 50*). We further removed the last 5bp of
159 each locus, SNPs heterozygous in at least 80% individuals, and loci with more than 5 SNPs. We

160 finally filtered all missing data by applying the *-minInd* filter equal to the total number of individual
161 present in each sampling site (Table 1). We then created a *site allele frequency likelihood (saf)* file
162 by using the SAMtools genotype likelihood computation method with the *-GL=1* flag (Li &
163 Durbin, 2009) and finally computed the folded *site frequency spectrum (SFS)* from the *saf* files
164 using the *RealSFS* program implemented in *ANGSD*. We computed the mean pairwise difference
165 (θ_π), the number of segregating sites (Watterson's Theta, θ_w) and Tajima's D (*TD*) directly from
166 the SFS. θ_π and θ_w were standardized per site (i.e., by taking into account both monomorphic and
167 polymorphic loci) and significance of *TD* was evaluated under 1,000 coalescent simulations of a
168 constant population model with size θ_π .

169

170 [Range Expansion](#)

171 Genetic diversity, here measured in each sampling site as θ_π , is expected to decay as a function of
172 the distance from the origin of the range expansion (Ramachandran et al., 2005). Geographic
173 distances were computed in order to take into account ecological features as it may better represent
174 the capacity of individuals to move between two points than linear distances. To that end, we
175 constructed a raster of 67894 cells using the R package *raster* (Hijmans, 2020) where each cell
176 corresponds either to land, open sea, seamount or reef habitat. Permeability coefficients were fixed
177 respectively to 0 and 1 for land and open sea, whereas coefficients for coral reefs and seamounts
178 were varied between 1 and 100. We applied two constraints: coral reefs should always have the
179 maximum relative permeability value (since they represent the only habitat for *C. amblyrhynchos*)
180 and seamounts have permeability bounded within 1 and coral reefs' value. The most likely values
181 were searched using a custom R script by maximising the correlation between the geographic and
182 genetic distances between the sampled sites. Geographic distances were computed with the

183 *gdistance* R package under the *Least Cost* (LC) criterion algorithm (van Etten, 2017) and genetic
184 distances were measured by the F_{ST} (see below). After this step, we considered each marine cells
185 of the raster to be a potential source of origin of the range expansion (RE) and computed its
186 distance from the sampled sites under the LC criterion with the most likely permeability values
187 previously estimated. We correlated these distances with the genetic diversity of each sampling
188 site to identify areas with more negative values, which are likely associated with the origin of the
189 RE (Ramachandran et al., 2005). We limited these analyses to the PAC sites to avoid possible bias
190 due to the gap in our sampling distribution (i.e., the lack of samples between IND and the
191 westernmost PAC site). Nevertheless, we verified the robustness of our results to the inclusion of
192 IND sites.

193

194 [Historical demographic inferences](#)

195 To account and test for meta-population structure, we performed model selection as well as
196 parameters estimation using an Approximate Bayesian Computation (ABC) framework
197 (Bertorelle, Benazzo, & Mona, 2010). We tested three demographic scenarios (Figure 2) for each
198 sampling site, namely NS, FIM, and SST. *Model NS (no structure)*: going backward in time, NS
199 represents a panmictic population where the effective population size switches instantaneously at
200 T_c generations from N_{mod} to N_{anc} . *Model FIM (Finite Island Model)*: FIM represents a meta-
201 population composed of a two-dimensional array of 10x10 demes (D_i), each of the same size N
202 that exchanges Nm migrants with any other deme each generation. Going backward in time all
203 demes merge into a single population of size N_{anc} at T_{col} generations. *Model SST (Stepping Stone)*:
204 SST is similar to FIM but demes exchange migrants only with their four closest neighbours. We
205 performed 50000 simulations under each scenario and for each sampling site independently using

206 *fastsimcoal2* (Excoffier & Foll, 2011). We run the model selection with the Random Forest
207 classification method implemented in the package *abcRF* (Pudlo et al., 2016) using the SFS, θ_π ,
208 θ_w and *TD* as summary statistics, to which we added the first two components of the Linear
209 Discriminant Analysis performed on the previous summary statistics as suggested by Pudlo et al.
210 (2016) to increase accuracy. We performed 50000 additional simulations under the most supported
211 scenario in order to estimate the demographic parameters using the *abcRF* regression method
212 (Raynal et al., 2019) with the same summary statistics as for the model selection. For all analyses,
213 we performed the estimation twice to check for the consistency of the inferences. The number of
214 trees was chosen by checking the out-of-bag error rate (OOB), and cross validation was performed
215 for both parameter inference and model selection (hereafter, the confusion matrix) procedures. We
216 finally modelled the variation of effective population size (N_e) through time in each sampling site
217 with the *stairwayplot* (Liu & Fu, 2015). The *stairwayplot* assumes that the sampled lineages come
218 from an isolated (panmictic) population (i.e., *unstructured*), which is not true in our case (see
219 results). However, this method allows a powerful investigation of the underlying gene genealogy
220 which provides useful elements for interpreting the evolutionary history of a meta-population
221 (Lesturgie et al., 2022). All demographic inferences were performed using a generation time of 10
222 years and a mutation rate of $1.93e-8$ per generation and per site following Lesturgie et al. (2022).

223

224 Population structure

225 Population structure inferences were performed on the dataset obtained following the assembly
226 pipeline implemented in *Stacks 2.5* as described above. After the *de novo* assembly step, the
227 *population* script was called to keep loci present in at least 80% of the individuals per sampling
228 site ($r = 0.8$) and with a *minor allele frequency* of 0.05, hence removing low frequency variants.

229 We finally retained one random SNP per locus. Using a custom R script, we further filtered: (i)
230 SNPs heterozygotes in more than 80% of the sample; (ii) loci with coverage higher than ~30x
231 (which corresponds to the mean coverage plus twice the standard deviation); (iii) SNPs in the last
232 5bp of the assembled locus; and (iv) loci containing more than five SNPs, after visual inspection
233 of the distribution of segregating sites per locus. The resulting dataset was used for the following
234 analyses. 1) *sNMF* implemented in the R package *LEA* (Frichot & François, 2015): we investigated
235 the number of ancestral clusters K by running the algorithm 10 times, with values of K ranging
236 from 1 to 8. We chose the most likely K using the cross-entropy criterion and displayed the
237 admixture coefficients under the best run. 2) *DAPC* implemented in the R package *Adegenet*
238 (Jombart, Devillard, & Balloux, 2010): we varied K from 1 to 8 and chose the best values based
239 on the BIC criterion. Linear discriminant functions were used to test whether individuals were
240 correctly reassigned to the inferred clusters. 3) F_{ST} : we computed overall and pairwise F_{ST} between
241 sampling sites with more than 5 individuals using the *PopGenome* (flag *nucleotide.F_ST*) library
242 in R (Pfeifer, Wittelsbürger, Ramos-Onsins, & Lercher, 2014) and tested its significance with 1000
243 permutations using a custom R script. Isolation by distance (IBD) was computed with a Mantel
244 Test (Mantel, 1967) between the genetic ($F_{ST}/(1-F_{ST})$) and the geographic or LC distance matrices
245 and tested by 1000 permutations with the *ade4* R package (Thioulouse & Dray, 2007). The Mantel
246 test, similarly as before, was limited to PAC sites. To check for IBD in the Indian Ocean, we fit a
247 linear model to the pairwise F_{ST} values computed between the PAC and IND sites and their
248 respective geographic distances.

249 Results

250 Genetic diversity

251 We discarded 30 individuals based on an excess of missing data after an initial *de novo* assembly.
252 We found a mean depth of coverage of 10.77x (s.d. = 2.32) for the whole dataset. Summary
253 statistics for all sampling sites are displayed in Table 1. The number of loci (monomorphic
254 included) and SNPs with no missing data ranged from 35594 to 146858 and from 36982 to 103258
255 respectively across sampling sites (Table 1). Genetic diversity (θ_π and θ_w) was lower in IND
256 sampling sites than in PAC (Table 1). Tajima's *D* values were positive in IND sampling sites and
257 in Fakarava, suggesting an excess of high frequency variants when compared to the standard
258 neutral model. Conversely, we found negative and significant Tajima's *D* values in all other PAC
259 locations (except for Moorea and Mckean), suggesting an excess of low frequency variants
260 compared to the standard neutral model (Table 1).

261

262 Range Expansion

263 The permeability coefficients maximising the correlation between genetic and the LC distances
264 were very similar between the three habitat types. Indeed, we estimated the values of 1:1.02:1.02
265 for open sea, coral reef habitat and seamounts respectively. These values were retained for the
266 following RE and IBD analyses. We plotted the correlation map computed using PAC sites only
267 in Figure 3. The most negative correlation coefficients are concentrated close to the COR sampling
268 sites, suggesting that the most likely origin of the RE is slightly east to the IAA region (Figure 3).
269 We found consistent results when adding IND sites to the analysis (Figure S1), despite the
270 geographic unbalanced distribution of our samples.

271

272 Historical demographic inferences

273 We investigated the demographic history for all sampling sites with $n \geq 7$. We first used an ABC-
274 RF framework to compare demographic scenarios (Figure 2). SST was the most supported scenario
275 in all locations, with posterior probabilities ranging from 0.48 to 0.78 and similar classification
276 error rate among locations (Table 2 and S1). The median Nm ranged from ~ 6 to ~ 14 (Table 2).
277 Posterior distributions of Nm were overlapping and clearly distinct from the prior distribution
278 (Figure S2), and both the squared mean error (SME) and the mean root squared error (MRSE)
279 were small among locations, suggesting reliable estimates (Table S2). Posterior distributions of
280 T_{col} overlapped among locations (Figure S2). Juan de Nova displayed a lower N_{anc} median value
281 ($\sim 21k$) than PAC sampling sites (ranging from $\sim 34k$ to $\sim 50k$) although all credible intervals
282 overlapped (Figure S2 and Table 2). Surprisingly, the ABC estimates of T_{col} and N_{anc} for the
283 Mckean sampling site were inconsistent with any other PHO sampling sites (Figure S2 and Table
284 2). However, both SME and the MRSE for these two parameters were generally one order of
285 magnitude larger than those estimated for Nm in all sampling sites (Table S2), suggesting less
286 accurate estimates for T_{col} and N_{anc} .

287 We further investigated the variation of N_e through time using the *stairwayplot* algorithm (Figure
288 4). We detected a broadly similar N_e dynamic across sampling sites that we summarized for
289 simplicity in three time periods: looking forward in time we observed an ancestral expansion
290 followed by a constant phase and a final systematic strong decrease in recent times (Figure 4).
291 However, we found three main differences between IND and PAC sampling sites: i) the expansion
292 time was around twice as recent in IND than in PAC ($\sim 180ky$ B.P. vs. $\sim 400ky$ B.P); ii) the strength
293 of the expansion is much stronger in PAC sampling sites; iii) N_e during the constant period reached
294 a value of ~ 40000 in PAC sampling sites and of only ~ 20000 in IND, consistent with the computed

295 θ (Table 1). The PAC sampling sites showed a remarkably homogeneous *stairwayplot*, with only
296 the peripheral sites (Fakarava and Palmyra) having a slightly more recent ancestral expansion
297 (Figure 4).

298

299 Population structure

300 After filtering, 88276 variable loci were retained to perform individual based structure analyses.
301 Both *sNMF* and the *DAPC* clustering algorithms found $K=2$ as the most likely number of ancestral
302 populations or clusters (Figure S3 and S4a). The ancestral populations inferred by *sNMF* perfectly
303 matched the two oceanic regions, namely the Indian and the Pacific Ocean: the ancestry proportion
304 of *cluster 1* in IND samples ranged from 70% to 100% while the ancestry proportion of *cluster 2*
305 in PAC samples ranged from 87% to 100% (Figure 5a). This highlights slightly more admixture
306 in IND than in PAC samples. We retained one LD function in the *DAPC* which correctly re-
307 assigned all individuals from IND and PAC to *cluster 1* and *cluster 2* respectively (Figure S4b).
308 We further investigated $K=3$ under both algorithms and found three main results: i) the ancestral
309 populations or clusters clearly identify three geographic areas corresponding to IND, COR, and
310 CPA regions (Figure 5a and S5); ii) the ancestry proportion of *cluster 3* follows a clinal
311 distribution, steadily increasing in frequency from West (Indian Ocean) to East (French Polynesia)
312 (Figure 5a); iii) all individuals belonging to the three areas are correctly re-assigned to the three
313 clusters by the *DAPC* computed with two LD functions (Figure S4b). We then computed a PCA
314 which showed similar results, with the first principal component explaining ~14.5% of the total
315 variance and clearly separating individuals coming from the two oceans (Figure 5b). The second
316 axis segregated CPA from COR samples. In agreement with the cluster analyses, CPA and COR
317 are only slightly differentiated as the second principal component explains only ~1% of the total

318 variance. The second axis also suggested a clinal differentiation between the two clusters (Figure
319 5b).

320 Population based analyses were performed on a reduced dataset excluding sampling sites with less
321 than $n=5$ individuals. We therefore retained 14 sampling sites, $n=168$ individuals, and 88824
322 variable loci and obtained an overall $F_{ST} = 0.25$ ($p\text{-value} < 0.001$). The pairwise F_{ST} highlighted a
323 strong differentiation between Indian and Pacific sampling sites with values ranging from 0.53 to
324 0.56 (and always significant, $p\text{-value} \leq 0.001$, Table S3). In contrast, comparisons within oceanic
325 regions never exceed 0.03 (Figure 6a) with values not always statistically significant. Consistently
326 with clustering results, a heatmap displaying pairwise F_{ST} values visually suggest the existence of
327 the three clusters previously identified (Figure 6a). However, the average differentiation between
328 COR and CPA is only slightly higher than within group comparisons (Figure 6a). Moreover, we
329 found a strong signature of isolation by distance (IBD) within the Pacific Ocean (using PAC sites
330 only), since the correlation between the F_{ST} and geographic or LC distance matrices was high and
331 significant (Mantel test: $r = 0.93$; $p\text{-value} < 0.001$ in both cases, Figure 6b). The correlation
332 between genetic and geographic distances by considering only IND vs. PAC pairwise distances
333 was also considerable although lower than in PAC region only ($r = 0.77$, Figure S5).

334 Discussion

335 Range expansion

336 Range expansions (RE) occur by a series of founder effects leading to the fixation of novel alleles
337 and the decay in genetic diversity as colonization progresses (Excoffier, Foll, & Petit, 2009). They
338 also leave specific signatures in the gene genealogy of lineages sampled from a deme of the meta-
339 population (Maisano Delser et al., 2016; Ray, Currat, & Excoffier, 2003) and in the extent of
340 population structure (Mona, 2017; Mona, Ray, Arenas, & Excoffier, 2014). Testing for the

341 occurrence of a RE is therefore fundamental to understanding the evolutionary history of a species.
342 Here, the spatial distribution of genetic diversity suggested the occurrence of a RE most likely
343 starting east of the Indo-Australian Archipelago (IAA). The inferred origin area was large (Figure
344 3), likely due to low differences in θ_π between Pacific sampling sites (Table 1), but robust to the
345 inclusion of samples from the Indian Ocean (Figure S1). The scenario of a RE was corroborated
346 by other evidence. First, the strong and significant correlation coefficient between genetic and
347 geographic distances in the Pacific Ocean ($r=0.93$; Mantel p -value < 0.001 , Figure 6b and S5).
348 This result alone would not be conclusive, since a similar pattern is also expected under an
349 equilibrium isolation by distance, but it strengthens our previous findings. Second, the historical
350 demography inferences performed in each sampled deme showed that the pattern of genetic
351 variability was most likely the outcome of a non-equilibrium meta-population structured according
352 to a stepping stone migration matrix (Table 2). In this context, both the colonization times of the
353 meta-population estimated by the ABC (Figure S2) and the expansion times retrieved by the
354 *stairwayplot* (Figure 4) harbour the signature of the RE process (Lesturgie et al., 2022): the oldest
355 times are expected to be close to the centre of origin of the RE, while the more recent ones are
356 likely associated to the edge of the colonization wave(s). While the large variance in T_{col} estimated
357 by ABC does not allow for an accurate interpretation of the temporal dynamics of colonisation
358 through the Indo-Pacific, the expansion times highlighted by the *stairwayplot* are consistent with
359 the RE scenario. Indeed, all sampling sites display a simultaneous expansion time around ~ 400 ky
360 B.P. (Figure 4) except for Palmyra, Fakarava and Juan de Nova, which are the sites respectively
361 further east (Palmyra and Fakarava) and west (Juan de Nova) to the inferred origin of the RE. In
362 summary, all the evidence presented thus far point to an origin of *C. amblyrhynchos* east of IAA
363 (particularly, east of New Caledonia), from which two migration waves took place, one to the East

364 Pacific and the other to the Indian Ocean, with the Mozambique Channel being probably one of
365 the last areas to have been colonized.

366 Our hypothesis is in line with the recent results of Walsh et al. (2022), but they detected the origin
367 of the RE within rather than eastward the IAA, using a similar genetic diversity decay approach
368 on low-coverage RAD-seq data. However, Walsh et al. (2022) assembled loci with *PyRAD* (Eaton,
369 2014), whose calling algorithm requires high coverage data to correctly identify genotypes
370 (Rochette et al., 2019). When coverage is low, the direct call of genotypes is likely to skew the
371 SFS towards an excess of singletons. This leads to biases in both genetic diversity estimates and
372 downstream demographic inferences: genotype-free approaches such as those implemented in
373 *ANGSD* (Mona et al. in prep; Heller et al. 2021) should be therefore preferred, as we did in this
374 work. To demonstrate this bias, we carefully compared our results (obtained with *ANGSD*) to those
375 obtained by three assembly and calling pipelines (namely, *PyRAD* (Eaton, 2014), *Stacks* v.1.48
376 (Catchen, Hohenlohe, Bassham, Amores, & Cresko, 2013) and *Stacks* v.2.5 (Rochette et al., 2019),
377 see Supplementary Methods) using the Bampton sampling site as a test case. Bampton belongs to
378 the Chesterfield islands, one of the sites considered by Walsh et al. (2022), and it is therefore
379 expected to share their same demographic history. All three SFS displayed an excess of singletons
380 in comparison to the one inferred by *ANGSD* (Figure S6b), clearly determining not only a stronger
381 ancestral expansion but also the absence of the recent bottleneck when fed to the *stairwayplot*
382 algorithm (Figure S6a). We note that by using the generation time and mutation rate of Walsh et
383 al. (2022) (a mutation rate only relevant to exon capture data (Maisano Delser et al., 2016) thus
384 lower than the one estimated for RAD-seq data (Lesturgie et al., 2022)), the *Ne* variation
385 reconstructed by the *stairwayplot* applied to our *PyRAD* assembly was highly similar to the results
386 they obtained in their Chesterfield sampling sites (compare our Figure 6b with their Figure 3).

387 Consequently, we highlight that the SFS reported by (Walsh et al., 2022) is biased toward an excess
388 of low frequency variants, skewing their inferred genetic diversity and the subsequent
389 demographic modelling. In turn, this implies that their results (and conclusions) might need to be
390 revised using a pipeline that explicitly takes into account low-coverage data.

391 The RE scenario, characterized by a centre of origin and two independent colonization waves, is
392 similar to the one inferred for *C. melanopterus* by (Maisano Delser et al., 2019), a species whose
393 range distribution overlaps with that of the grey reef shark. However, the most likely origin of the
394 RE was located within the IAA for *C. melanopterus*, a well-known centre of origin for many teleost
395 fishes (Cowman & Bellwood, 2013), and a biodiversity hotspot (Allen, 2008). The difference
396 observed between *C. amblyrhynchos* and *C. melanopterus* could result from the more balanced
397 sampling scheme of (Maisano Delser et al., 2019), who could cover more homogeneously the
398 Indo-Pacific. More samples from the IAA will be needed to refine our estimates. More generally,
399 it will be interesting in the next future to explicitly investigate the role of the IAA for coral reef
400 biodiversity fauna and to reconstruct the colonisations routes in the Indo-Pacific, using population
401 genetics modelling applied to genomics data on multiple marine species to extract more general
402 patterns (see for example Delrieu-Trottin et al. (2020)).

403

404 [Historical demography](#)

405 The ABC framework not only provided another evidence in favour of a non-equilibrium meta-
406 population scenario through the model selection analysis, but also allowed us to further refine our
407 understanding of the evolutionary history of the grey reef shark. By analysing each deme
408 separately, we found an overlapping posterior distribution of Nm with an average mode of ~ 10
409 (Table 2 and Figure S2). *C. amblyrhynchos*, similarly to *C. melanopterus*, is strongly dependent

410 on reefs, whose distribution is not homogenous in the Indo-Pacific (Figure S7). We would have
411 expected the connectivity in each sampled deme to be highly correlated to the distribution of coral
412 reef in its neighbourhood, as it was previously observed in *C. melanopterus* (Maisano Delser et
413 al., 2019). However, the two species differ in their dispersal behaviours: while grey reef sharks
414 perform long-distance movements of at least ~900 km (Barnett et al., 2012; Bonnin et al., 2019;
415 White et al., 2017), the blacktip reef shark exhibits a range of movement not exceeding ~50 km
416 (Johann Mourier & Planes, 2013). Our results reinforce the idea that the neighbourhood size in the
417 two species is very different, with *C. amblyrhynchos* being able to cross expanses of open ocean
418 and therefore being less sensitive to coral reef concentration than *C. melanopterus*.

419 The homogeneity in the signature of genetic variation in each deme was confirmed by the
420 *stairwayplot* analyses (Figure 4), contrasting with the heterogeneity previously described for *C.*
421 *melanopterus* (Maisano Delser et al., 2019). All demes showed an ancestral expansion followed
422 by a period of stasis and a strong bottleneck in recent times. We recently showed that these three
423 time periods are the typical signature of the variation in the coalescence rate through time due to
424 the meta-population structure, with the slight differences observed between sites being only due
425 to their specific colonization time (Lesturgie et al., 2022). This result confirms the similarity of
426 dispersal pattern throughout the Indo-Pacific. Similarly, the signature of bottleneck observed in
427 recent times for all demes (Figure 4) is also the expected consequence of population structure
428 (Chikhi et al., 2018; Lesturgie et al., 2022; Mazet et al., 2015; Rodríguez et al., 2018) and cannot
429 be interpreted as a demographic decline. Unfortunately, population structure and demographic
430 decline affect the SFS in a similar fashion making impossible to quantitatively disentangle the
431 contribution of both to the observed bottleneck estimated using RAD-seq data (Lesturgie et al.,
432 2022). We stress that investigating local recent changes in connectivity or demographic events will

433 clearly requires whole genome sequencing coupled with inferential methods based on the IICR
434 (Arredondo et al., 2021) and/or linkage disequilibrium (Boitard, Rodríguez, Jay, Mona, &
435 Austerlitz, 2016). More generally, the next challenge will be to perform a full modelling of species
436 structured in many demes as the grey reef shark. Here we took a simplified approach by
437 considering each sampling site separately and by modelling the unsampled demes to estimate local
438 migration rates. We are aware that in the future more data will be needed to explore complex
439 demographic scenarios integrating RE that include both all sampled demes and the unsampled
440 ones. In this light, the biological interpretation of parameters estimated under simplified models
441 discarding unsampled demes and ignoring RE (as in Walsh et al. (2022)) remains unclear.

442

443 [Population structure](#)

444 The results presented so far suggest that dispersal abilities of *C. amblyrhynchos* are similar
445 throughout the Indo-Pacific and independent of the availability of coral reefs. However, this cannot
446 exclude the presence of barriers to gene flow which may have shaped the connectivity between
447 demes. For widely distributed marine species, detecting such barriers may help to delineate
448 management units and to take proper conservation measures in relation to fisheries (Dudgeon et
449 al., 2012). Several evidence point to an absence of barriers to gene flow in the grey reef shark.
450 First of all, we found a strong IBD pattern with a significant correlation between genetic and
451 geographic distances of > 0.9 when considering only PAC samples (Figure 6b) and a linear relation
452 of smaller intensity between IND and PAC samples (Figure S5). Remarkably, these values are not
453 affected by computing geographic distances between sampling sites under an LC approach.
454 Indeed, the permeability values maximizing the correlation are (almost) the same for the different
455 type of habitats. This suggest that different geographic features do not affect the direction of grey

456 reef shark migrations, indicating, albeit indirectly, the absence of barriers to dispersal, consistently
457 with the occasional long-distance swims detected across the open ocean (Barnett et al., 2012;
458 Bonnin et al., 2019; White et al., 2017). When strong IBD is present, it is difficult to attribute a
459 biological meaning to groups identified by clustering algorithms (Meirmans, 2012). Both the
460 *sNMF* and PCA analyses suggested a strong separation between IND and PAC samples (Figure
461 5), with the latter subdivided into two weakly divergent clusters (Figure 5 and S8). The IND
462 ancestral components diminished remarkably continuously eastward, once again supporting an
463 IBD structure (Figure 5a) rather than the presence of barriers to gene flow. This is consistent with
464 the pairwise F_{ST} matrix, where intra Pacific comparisons did not exceed ~ 0.03 while the inter-
465 oceanic comparisons have an average F_{ST} of ~ 0.54 (Figure 6a). Defining management units within
466 the PAC seems therefore inappropriate in the case of the grey reef shark, as genetic variations are
467 rather continuous. This contrasts with what was previously suggested by Boissin et al. (2019) at
468 the Pacific scale: however, their results were based on a small number of microsatellites and they
469 did not model IBD between the sampling points.

470 The pitfall of our study is to extrapolate the dynamic of the grey reef shark at the scale of its whole
471 range by focusing mostly on the Pacific Ocean. Indeed, even if the species seems to follow an IBD
472 pattern also from Chagos to Eastern Australia (Momigliano et al., 2017), the level of population
473 differentiation appears to be higher than what we found in the Pacific for similar geographic
474 distances. However, while the distribution of coral reef in the Pacific Ocean is scattered due to the
475 presence of many archipelagos, coral reefs in the Indian Ocean are more concentrated on the
476 coastal edge of the Asian and African continents (Figure S7). The effective distance between
477 sampling sites within the Indian Ocean would therefore be larger than in the Pacific Ocean, where
478 coral reefs would act as stepping stones to facilitate the colonization process and further

479 migrations. This could also account for the different linear relationship estimated in the Pacific vs.
480 the one estimated between Pacific and Indian sampling sites (Figure S5).

481

482 Conclusion

483 We explored the evolutionary history of the grey reef shark throughout most of its range in the
484 Indo-Pacific and contrasted the results with those previously obtained for the blacktip reef shark
485 (Maisano Delser et al., 2019). The two species are among the most abundant reef sharks (MacNeil
486 et al., 2020), share an almost overlapping distribution in the Indo-Pacific and are both strictly coral
487 reef-dependent species. Despite similarities in the RE dynamic, patterns of genetic diversity and
488 population structure are very different between the two species. First, *C. melanopterus* is
489 significantly more structured than *C. amblyrhynchos* at similar spatial distances (for comparison,
490 F_{ST} values are ~30 times higher when comparing French Polynesia vs New Caledonia, see Table
491 S5 of Maisano Delser et al. (2019) and our Table S3). Second, *C. amblyrhynchos* shows
492 homogeneous migration rates and demographic signals throughout its whole distribution whereas
493 *C. melanopterus* is more sensitive to the spatial distribution of coral reef with a connectivity largely
494 dependent on the short scale reef-availability (Maisano Delser et al., 2019). Indeed, migration rates
495 estimated in areas with extensive coral reefs coverage (e.g., the Great Barrier Reef) are much
496 higher compared to those estimated in isolated islands/atolls in the Indo-Pacific (Maisano Delser
497 et al., 2019), something that we did not observe for *C. amblyrhynchos*. All these differences can
498 be explained by the life history traits related to dispersal abilities of the two species, with *C.*
499 *amblyrhynchos* moving more freely in open sea expanses compared to *C. melanopterus*, lowering
500 the impact of coral density on the observed genetic diversity. However, it will be important in the
501 next future to precisely characterize the extent of the neighbourhood size for both species. To this

502 end, ecological and genomic data need to be coupled: this will help to carefully decipher how many
503 management units are necessary for species conservation and at which scale they should be
504 established.

505 **Acknowledgement**

506 We are grateful to the Genotoul bioinformatics platform Toulouse Midi-Pyrenees (Bioinfo
507 Genotoul; <http://bioinfo.genotoul.fr/>) for providing computing resources. We are thankful to
508 Valeriano Parravicini for his input and for providing resources on coral reef distribution in the
509 Indo-Pacific and Romuald Laso-Jadart for critical reading. We thank Jenn Caselle and Darcy
510 Bradley for providing samples from the Phoenix archipelago. This work was supported by two
511 ATM grants (2016 and 2017) from the Muséum National d'Histoire Naturelle to S.M.

512 **Authors contribution**

513 S.M coordinated the study. P.L carried out data analysis with inputs from S.M. P.L. and S.M
514 conceived the study and wrote the paper. C.B., E.C., J.K., J.M., S.T., T.V. and S.P. collected
515 samples, provided reagents and revised the manuscript.

516 **Data archiving**

517 VCF files, SFS and scripts are available from the Dryad Digital Repository:
518 [doi:10.5061/dryad.547d7wm9b](https://doi.org/10.5061/dryad.547d7wm9b)_Fastq sequence files are available from the GenBank at the
519 National Center for Biotechnology Information short-read archive database (accession number:
520 forthcoming).

521

522

523 References

- 524 Allen, G. R. (2008). Conservation hotspots of biodiversity and endemism for Indo-Pacific coral
525 reef fishes. *Aquatic Conservation: Marine and Freshwater Ecosystems*, 18(5), 541–556.
526 <https://doi.org/10.1002/aqc.880>
- 527 Arredondo, A., Mourato, B., Nguyen, K., Boitard, S., Rodríguez, W., Noûs, C., ... Chikhi, L.
528 (2021). Inferring number of populations and changes in connectivity under the n-island
529 model. *Heredity*, 126(6), 896–912. <https://doi.org/10.1038/s41437-021-00426-9>
- 530 Bailleul, D., Mackenzie, A., Sacchi, O., Poisson, F., Bierne, N., & Arnaud-Haond, S. (2018).
531 Large-scale genetic panmixia in the blue shark (*Prionace glauca*): A single worldwide
532 population, or a genetic lag-time effect of the “grey zone” of differentiation? *Evolutionary*
533 *Applications*, 11(5), 614–630. <https://doi.org/10.1111/eva.12591>
- 534 Barnett, A., Abrantes, K. G., Seymour, J., & Fitzpatrick, R. (2012). Residency and spatial use by
535 reef sharks of an isolated seamount and its implications for conservation. *PLoS ONE*, 7(5),
536 1–12. <https://doi.org/10.1371/journal.pone.0036574>
- 537 Benazzo, A., Trucchi, E., Cahill, J. A., Delser, P. M., Mona, S., Fumagalli, M., ... Bertorelle, G.
538 (2017). Survival and divergence in a small group: The extraordinary genomic history of the
539 endangered Apennine brown bear stragglers. *Proceedings of the National Academy of*
540 *Sciences of the United States of America*, 114(45), E9589–E9597.
541 <https://doi.org/10.1073/pnas.1707279114>
- 542 Bertorelle, G., Benazzo, A., & Mona, S. (2010). ABC as a flexible framework to estimate
543 demography over space and time: Some cons, many pros. *Molecular Ecology*, 19(13),
544 2609–2625. <https://doi.org/10.1111/j.1365-294X.2010.04690.x>
- 545 Boissin, E., Thorrold, S. R., Braun, C. D., Zhou, Y., Clua, E. E., & Planes, S. (2019). Contrasting

546 global, regional and local patterns of genetic structure in gray reef shark populations from
547 the Indo-Pacific region. *Scientific Reports*, 9(1), 1–9. [https://doi.org/10.1038/s41598-019-](https://doi.org/10.1038/s41598-019-52221-6)
548 52221-6

549 Boitard, S., Rodríguez, W., Jay, F., Mona, S., & Austerlitz, F. (2016). Inferring Population Size
550 History from Large Samples of Genome-Wide Molecular Data - An Approximate Bayesian
551 Computation Approach. *PLOS Genetics*, 12(3), e1005877.
552 <https://doi.org/10.1371/journal.pgen.1005877>

553 Bonnin, L., Robbins, W. D., Boussarie, G., Kiszka, J. J., Dagorn, L., Mouillot, D., & Vigliola, L.
554 (2019). Repeated long-range migrations of adult males in a common Indo-Pacific reef
555 shark. *Coral Reefs*, 38(6), 1121–1132. <https://doi.org/10.1007/s00338-019-01858-w>

556 Bornatowski, H., Navia, A. F., Braga, R. R., Abilhoa, V., & Corrêa, M. F. M. (2014). Ecological
557 importance of sharks and rays in a structural foodweb analysis in southern Brazil. *ICES*
558 *Journal of Marine Science*, 71(7), 1586–1592. <https://doi.org/10.1093/icesjms/fsu025>

559 Catchen, J., Hohenlohe, P. A., Bassham, S., Amores, A., & Cresko, W. A. (2013). Stacks: an
560 analysis tool set for population genomics. *Molecular Ecology*, 22(11), 3124–3140.
561 <https://doi.org/10.1111/mec.12354>

562 Chikhi, L., Rodríguez, W., Grusea, S., Santos, P., Boitard, S., & Mazet, O. (2018). The IICR
563 (inverse instantaneous coalescence rate) as a summary of genomic diversity: Insights into
564 demographic inference and model choice. *Heredity*, 120(1), 13–24.
565 <https://doi.org/10.1038/s41437-017-0005-6>

566 Chikhi, L., Sousa, V. C., Luisi, P., Goossens, B., & Beaumont, M. A. (2010). The Confounding
567 Effects of Population Structure, Genetic Diversity and the Sampling Scheme on the
568 Detection and Quantification of Population Size Changes. *Genetics*, 186(3), 983–995.

569 <https://doi.org/10.1534/genetics.110.118661>

570 Compagno, L. J. . (2001). Sharks of the world. An annotated and illustrated catalogue of shark
571 species known to date. Volume 2. Bullhead, mackerel and carpet sharks
572 (Heterodontiformes, Lamniformes and Orectolobiformes). *FAO Species Catalogue for*
573 *Fishery Purposes*, 2(1), 108–125.

574 Corrigan, S., Lowther, A. D., Beheregaray, L. B., Bruce, B. D., Cliff, G., Duffy, C. A., ...
575 Rogers, P. J. (2018). Population Connectivity of the Highly Migratory Shortfin Mako
576 (*Isurus oxyrinchus* Rafinesque 1810) and Implications for Management in the Southern
577 Hemisphere. *Frontiers in Ecology and Evolution*, 6(NOV), 1–15.
578 <https://doi.org/10.3389/fevo.2018.00187>

579 Cowman, P. F., & Bellwood, D. R. (2013). The historical biogeography of coral reef fishes:
580 Global patterns of origination and dispersal. *Journal of Biogeography*, 40(2), 209–224.
581 <https://doi.org/10.1111/jbi.12003>

582 Delrieu-Trottin, E., Hubert, N., Giles, E. C., Chifflet-Belle, P., Suwalski, A., Neglia, V., ...
583 Saenz-Agudelo, P. (2020). Coping with Pleistocene climatic fluctuations: Demographic
584 responses in remote endemic reef fishes. *Molecular Ecology*, 29(12), 2218–2233.
585 <https://doi.org/10.1111/mec.15478>

586 Dudgeon, C. L., Blower, D. C., Broderick, D., Giles, J. L., Holmes, B. J., Kashiwagi, T., ...
587 Ovenden, J. R. (2012). A review of the application of molecular genetics for fisheries
588 management and conservation of sharks and rays. *Journal of Fish Biology*, 80(5), 1789–
589 1843. <https://doi.org/10.1111/j.1095-8649.2012.03265.x>

590 Dulvy, N. K., Pacoureau, N., Rigby, C. L., Pollom, R. A., Jabado, R. W., Ebert, D. A., ...
591 Simpfendorfer, C. A. (2021). Overfishing drives over one-third of all sharks and rays

592 toward a global extinction crisis. *Current Biology*, 1–15.
593 <https://doi.org/10.1016/j.cub.2021.08.062>

594 Dwyer, R. G., Krueck, N. C., Udyawer, V., Heupel, M. R., Chapman, D., Pratt, H. L., ...
595 Simpfendorfer, C. A. (2020). Individual and Population Benefits of Marine Reserves for
596 Reef Sharks. *Current Biology*, 30(3), 480–489.e5. <https://doi.org/10.1016/j.cub.2019.12.005>

597 Eaton, D. A. R. (2014). PyRAD: Assembly of de novo RADseq loci for phylogenetic analyses.
598 *Bioinformatics*, 30(13), 1844–1849. <https://doi.org/10.1093/bioinformatics/btu121>

599 Espinoza, M., Heupel, M. R., Tobin, A. J., & Simpfendorfer, C. A. (2014). Residency patterns
600 and movements of grey reef sharks (*Carcharhinus amblyrhynchos*) in semi-isolated coral
601 reef habitats. *Marine Biology*, 162(2), 343–358. <https://doi.org/10.1007/s00227-014-2572-x>

602 Excoffier, L., & Foll, M. (2011). fastsimcoal: A continuous-time coalescent simulator of
603 genomic diversity under arbitrarily complex evolutionary scenarios. *Bioinformatics*, 27(9),
604 1332–1334. <https://doi.org/10.1093/bioinformatics/btr124>

605 Excoffier, L., Foll, M., & Petit, R. J. (2009). Genetic Consequences of Range Expansions.
606 *Annual Review of Ecology, Evolution, and Systematics*, 40(1), 481–501.
607 <https://doi.org/10.1146/annurev.ecolsys.39.110707.173414>

608 Field, I. C., Meekan, M. G., Speed, C. W., White, W., & Bradshaw, C. J. A. (2011). Quantifying
609 movement patterns for shark conservation at remote coral atolls in the Indian Ocean. *Coral*
610 *Reefs*, 30(1), 61–71. <https://doi.org/10.1007/s00338-010-0699-x>

611 Frichot, E., & François, O. (2015). LEA: An R package for landscape and ecological association
612 studies. *Methods in Ecology and Evolution*, 6(8), 925–929. [https://doi.org/10.1111/2041-](https://doi.org/10.1111/2041-210X.12382)
613 [210X.12382](https://doi.org/10.1111/2041-210X.12382)

614 Friedlander, A. M., & DeMartini, E. E. (2002). Contrasts in density, size, and biomass of reef

615 fishes between the northwestern and the main Hawaiian islands: The effects of fishing down
616 apex predators. *Marine Ecology Progress Series*, 230, 253–264.
617 <https://doi.org/10.3354/meps230253>

618 Heled, J., & Drummond, A. J. (2008). Bayesian inference of population size history from
619 multiple loci. *BMC Evolutionary Biology*, 8(1), 289. [https://doi.org/10.1186/1471-2148-8-](https://doi.org/10.1186/1471-2148-8-289)
620 289

621 Heller, R., Chikhi, L., & Siegismund, H. R. (2013). The Confounding Effect of Population
622 Structure on Bayesian Skyline Plot Inferences of Demographic History. *PLoS ONE*, 8(5).
623 <https://doi.org/10.1371/journal.pone.0062992>

624 Heller, R., Nursyifa, C., Garcia-Erill, G., Salmons, J., Chikhi, L., Meisner, J., ... Albrechtsen, A.
625 (2021). A reference-free approach to analyse RADseq data using standard next generation
626 sequencing toolkits. *Molecular Ecology Resources*, 21(4), 1085–1097.
627 <https://doi.org/10.1111/1755-0998.13324>

628 Hijmans, R. J. (2020). *Raster: Geographic Data Analysis and Modeling*.

629 Jombart, T., Devillard, S., & Balloux, F. (2010). Discriminant analysis of principal components:
630 A new method for the analysis of genetically structured populations. *BMC Genetics*, 11(1),
631 94. <https://doi.org/10.1186/1471-2156-11-94>

632 Khimoun, A., Doums, C., Molet, M., Kaufmann, B., Peronnet, R., Eyer, P. A., & Mona, S.
633 (2020). Urbanization without isolation: The absence of genetic structure among cities and
634 forests in the tiny acorn ant *Temnothorax nylanderi*. *Biology Letters*, 16(1).
635 <https://doi.org/10.1098/rsbl.2019.0741>

636 Korneliussen, T. S., Albrechtsen, A., & Nielsen, R. (2014). ANGSD: Analysis of Next
637 Generation Sequencing Data. *BMC Bioinformatics*, 15(1), 1–13.

638 <https://doi.org/10.1186/s12859-014-0356-4>

639 Lesturgie, P., Planes, S., & Mona, S. (2022). Coalescence times, life history traits and
640 conservation concerns: An example from four coastal shark species from the Indo-Pacific.
641 *Molecular Ecology Resources*, 22(2), 554–566. <https://doi.org/10.1111/1755-0998.13487>

642 Li, H., & Durbin, R. (2009). Fast and accurate short read alignment with Burrows-Wheeler
643 transform. *Bioinformatics*, 25(14), 1754–1760.
644 <https://doi.org/10.1093/bioinformatics/btp324>

645 Li, H., & Durbin, R. (2011). Inference of human population history from individual whole-
646 genome sequences. *Nature*, 475(7357), 493–496. <https://doi.org/10.1038/nature10231>

647 Liu, X., & Fu, Y.-X. (2015). Exploring population size changes using SNP frequency spectra.
648 *Nature Genetics*, 47(5), 555–559. <https://doi.org/10.1038/ng.3254>

649 MacNeil, M. A., Chapman, D. D., Heupel, M., Simpfendorfer, C. A., Heithaus, M., Meekan, M.,
650 ... Cinner, J. E. (2020). Global status and conservation potential of reef sharks. *Nature*,
651 583(7818), 801–806. <https://doi.org/10.1038/s41586-020-2519-y>

652 Maisano Delser, P., Corrigan, S., Duckett, D., Suwalski, A., Veuille, M., Planes, S., ... Mona, S.
653 (2019). Demographic inferences after a range expansion can be biased: the test case of the
654 blacktip reef shark (*Carcharhinus melanopterus*). *Heredity*, 122(6), 759–769.
655 <https://doi.org/10.1038/s41437-018-0164-0>

656 Maisano Delser, P., Corrigan, S., Hale, M., Li, C., Veuille, M., Planes, S., ... Mona, S. (2016).
657 Population genomics of *C. melanopterus* using target gene capture data: Demographic
658 inferences and conservation perspectives. *Scientific Reports*, 6(April), 1–12.
659 <https://doi.org/10.1038/srep33753>

660 Mantel, N. (1967). The Detection of Disease Clustering and a Generalized Regression Approach.

661 *Cancer Research*, 27(2), 209–220.

662 Mazet, O., Rodríguez, W., Grusea, S., Boitard, S., & Chikhi, L. (2016). On the importance of
663 being structured: instantaneous coalescence rates and human evolution—lessons for
664 ancestral population size inference? *Heredity*, 116(4), 362–371.
665 <https://doi.org/10.1038/hdy.2015.104>

666 Mazet, O, Rodríguez, W., & Chikhi, L. (2015). Demographic inference using genetic data from a
667 single individual: Separating population size variation from population structure.
668 *Theoretical Population Biology*, 104, 46–58. <https://doi.org/10.1016/j.tpb.2015.06.003>

669 Meirmans, P. G. (2012). The trouble with isolation by distance. *Molecular Ecology*, 21(12),
670 2839–2846. <https://doi.org/10.1111/j.1365-294X.2012.05578.x>

671 Momigliano, P., Harcourt, R., Robbins, W. D., Jaiteh, V., Mahardika, G. N., Sembiring, A., &
672 Stow, A. (2017). Genetic structure and signatures of selection in grey reef sharks
673 (*Carcharhinus amblyrhynchos*). *Heredity*, 119(3), 142–153.
674 <https://doi.org/10.1038/hdy.2017.21>

675 Momigliano, P., Harcourt, R., Robbins, W. D., & Stow, A. (2015). Connectivity in grey reef
676 sharks (*Carcharhinus amblyrhynchos*) determined using empirical and simulated genetic
677 data. *Scientific Reports*, 5(August), 1–9. <https://doi.org/10.1038/srep13229>

678 Mona, S. (2017). On the role played by the carrying capacity and the ancestral population size
679 during a range expansion. *Heredity*, 118(2), 143–153. <https://doi.org/10.1038/hdy.2016.73>

680 Mona, S., Ray, N., Arenas, M., & Excoffier, L. (2014). Genetic consequences of habitat
681 fragmentation during a range expansion. *Heredity*, 112(3), 291–299.
682 <https://doi.org/10.1038/hdy.2013.105>

683 Mourier, J., Mills, S. C., & Planes, S. (2013). Population structure, spatial distribution and life-

684 history traits of blacktip reef sharks *Carcharhinus melanopterus*. *Journal of Fish Biology*,
685 82(3), 979–993. <https://doi.org/10.1111/jfb.12039>

686 Mourier, Johann, & Planes, S. (2013). Direct genetic evidence for reproductive philopatry and
687 associated fine-scale migrations in female blacktip reef sharks (*Carcharhinus melanopterus*)
688 in French Polynesia. *Molecular Ecology*, 22(1), 201–214.
689 <https://doi.org/10.1111/mec.12103>

690 Myers, R. A., Baum, J. K., Shepherd, T. D., Powers, S. P., & Peterson, C. H. (2007). Cascading
691 effects of the loss of apex predatory sharks from a coastal ocean. *Science*, 315(5820), 1846–
692 1850. <https://doi.org/10.1126/science.1138657>

693 Pazmiño, D. A., Maes, G. E., Green, M. E., Simpfendorfer, C. A., Hoyos-Padilla, E. M., Duffy,
694 C. J. A., ... Van Herwerden, L. (2018). Strong trans-Pacific break and local conservation
695 units in the Galapagos shark (*Carcharhinus galapagensis*) revealed by genome-wide
696 cytonuclear markers. *Heredity*, 120(5), 407–421. [https://doi.org/10.1038/s41437-017-0025-](https://doi.org/10.1038/s41437-017-0025-2)
697 2

698 Peterson, B. K., Weber, J. N., Kay, E. H., Fisher, H. S., & Hoekstra, H. E. (2012). Double Digest
699 RADseq: An Inexpensive Method for De Novo SNP Discovery and Genotyping in Model
700 and Non-Model Species. *PLoS ONE*, 7(5), e37135.
701 <https://doi.org/10.1371/journal.pone.0037135>

702 Pfeifer, B., Wittelsbürger, U., Ramos-Onsins, S. E., & Lercher, M. J. (2014). PopGenome: An
703 efficient swiss army knife for population genomic analyses in R. *Molecular Biology and*
704 *Evolution*, 31(7), 1929–1936. <https://doi.org/10.1093/molbev/msu136>

705 Pirog, A., Jaquemet, S., Ravigné, V., Cliff, G., Clua, E., Holmes, B. J., ... Magalon, H. (2019).
706 Genetic population structure and demography of an apex predator, the tiger shark

707 Galeocerdo cuvier. *Ecology and Evolution*, 9(10), 5551–5571.
708 <https://doi.org/10.1002/ece3.5111>

709 Pudlo, P., Marin, J.-M. M., Estoup, A., Cornuet, J.-M. M., Gautier, M., & Robert, C. P. (2016).
710 Reliable ABC model choice via random forests. *Bioinformatics*, 32(6), 859–866.
711 <https://doi.org/10.1093/bioinformatics/btv684>

712 Ramachandran, S., Deshpande, O., Roseman, C. C., Rosenberg, N. A., Feldman, M. W., &
713 Cavalli-Sforza, L. L. (2005). Support from the relationship of genetic and geographic
714 distance in human populations for a serial founder effect originating in Africa. *Proceedings*
715 *of the National Academy of Sciences*, 102(44), 15942–15947.
716 <https://doi.org/10.1073/pnas.0507611102>

717 Ray, N., Currat, M., & Excoffier, L. (2003). Intra-deme molecular diversity in spatially
718 expanding populations. *Molecular Biology and Evolution*, 20(1), 76–86.
719 <https://doi.org/10.1093/molbev/msg009>

720 Raynal, L., Marin, J. M., Pudlo, P., Ribatet, M., Robert, C. P., & Estoup, A. (2019). ABC
721 random forests for Bayesian parameter inference. *Bioinformatics*, 35(10), 1720–1728.
722 <https://doi.org/10.1093/bioinformatics/bty867>

723 Robbins, W. D., Hisano, M., Connolly, S. R., & Choat, J. H. (2006). Ongoing Collapse of Coral-
724 Reef Shark Populations. *Current Biology*, 16(23), 2314–2319.
725 <https://doi.org/10.1016/j.cub.2006.09.044>

726 Rochette, N. C., Rivera-Colón, A. G., & Catchen, J. M. (2019). Stacks 2: Analytical methods for
727 paired-end sequencing improve RADseq-based population genomics. *Molecular Ecology*,
728 28(21), 4737–4754. <https://doi.org/10.1111/mec.15253>

729 Rodríguez, W., Mazet, O., Grusea, S., Arredondo, A., Corujo, J. M., Boitard, S., & Chikhi, L.

730 (2018). The IICR and the non-stationary structured coalescent: towards demographic
731 inference with arbitrary changes in population structure. *Heredity*, *121*(6), 663–678.
732 <https://doi.org/10.1038/s41437-018-0148-0>

733 Speed, C. W., Meekan, M. G., Field, I. C., McMahon, C. R., Harcourt, R. G., Stevens, J. D., ...
734 Bradshaw, C. J. A. (2016). Reef shark movements relative to a coastal marine protected
735 area. *Regional Studies in Marine Science*, *3*, 58–66.
736 <https://doi.org/10.1016/j.rsma.2015.05.002>

737 Steiner, C. C., Putnam, A. S., Hoeck, P. E. A., & Ryder, O. A. (2013). Conservation Genomics
738 of Threatened Animal Species. *Annual Review of Animal Biosciences*, *1*(1), 261–281.
739 <https://doi.org/10.1146/annurev-animal-031412-103636>

740 Thioulouse, J., & Dray, S. (2007). Interactive multivariate data analysis in R with the ade4 and
741 ade4TkGUI packages. *Journal of Statistical Software*, *22*(5), 1–14.
742 <https://doi.org/10.18637/jss.v022.i05>

743 van Etten, J. (2017). R package gdistance: Distances and routes on geographical grids. *Journal of*
744 *Statistical Software*, *76*(1). <https://doi.org/10.18637/jss.v076.i13>

745 Walsh, C. A. J., Momigliano, P., Boussarie, G., Robbins, W. D., Bonnin, L., Fauvelot, C., ...
746 Manel, S. (2022). *Genomic insights into the historical and contemporary demographics of*
747 *the grey reef shark*. (February). <https://doi.org/10.1038/s41437-022-00514-4>

748 White, T. D., Carlisle, A. B., Kroodsmas, D. A., Block, B. A., Casagrandi, R., De Leo, G. A., ...
749 McCauley, D. J. (2017). Assessing the effectiveness of a large marine protected area for
750 reef shark conservation. *Biological Conservation*, *207*, 64–71.
751 <https://doi.org/10.1016/j.biocon.2017.01.009>

752 Whitney, N. M., Robbins, W. D., Schultz, J. K., Bowen, B. W., & Holland, K. N. (2012).

753 Oceanic dispersal in a sedentary reef shark (*Triaenodon obesus*): Genetic evidence for
754 extensive connectivity without a pelagic larval stage. *Journal of Biogeography*, 39(6),
755 1144–1156. <https://doi.org/10.1111/j.1365-2699.2011.02660.x>

756

757

758

Tables

Table 1. Summary Statistics. Sample size (n), total number of loci (monomorphic included) (n_{loci}) and SNPs (n_{SNP}), mean pairwise difference (θ_{π}), Watterson theta (θ_w), Tajima's D (TD) for all sampling sites (ranged from west to east).

Region	Group	Sampling site	n	n_{loci}	n_{SNP}	θ_{π}^{\dagger}	θ_w^{\dagger}	TD [‡]
IND	IND	Juan	13	95027	45635	1.18	1.09	0.32
		Zelee	6	146858	62674	1.30	1.23	0.26
COR [§]	CHE	Bampton	10	89958	82869	2.14	2.26	-0.22
		Avond	5	125710	87817	2.10	2.15	-0.12
	NCA	Belep	7	120038	103258	2.30	2.35	-0.11
		Poindimie	5	107464	72995	2.07	2.09	-0.05
CPA [§]	PHO	Niku	21	49922	53349	2.02	2.16	-0.25
		McKean	7	112711	88258	2.13	2.14	-0.01
		Orona	11	81725	75423	2.15	2.20	-0.09
		Kanton	10	99720	87202	2.12	2.14	-0.05
		Birnie [¶]	2	-	-	-	-	-
	PAL	Enderbury	13	76314	72221	2.09	2.16	-0.12
		Palmyra	38	35594	36982	1.66	1.84	-0.35
		Moorea	5	104050	68380	2.03	2.02	0.02
		Fakarava	17	71715	66559	2.01	1.97	0.08
		POL	Faaite [¶]	1	-	-	-	-
Raraka [¶]	1		-	-	-	-	-	
Nengo [¶]	1		-	-	-	-	-	

[†] Mean pairwise difference and Watterson theta are expressed per site and are multiplied by a 10^3 factor.

[‡] Tajima's D values in bold are significant ($P < 0.001$).

[§] COR and CPA regions are from the Pacific Ocean (PAC).

[¶] Summary statistics were not computed in sampling sites with $n < 5$.

Table 2. ABC estimation. Posterior probability (PP) of the Stepping Stone model (SST) and its parameters (median value and 95% credible interval in parentheses).

Region	Group	Sampling site	PP	Nm	T_{col}	N_{anc}
IND	IND	Juan	0.67	5.7	257800	21086
				(1.77 - 17.72)	(8086 - 658471)	(399 - 52652)
COR [§]	CHE	Bampton	0.73	11.41	188782	45965
				(3.97 - 19.03)	(127761 - 577503)	(27556 - 49856)
	NCA	Belep	0.51	7.8	241218	49239
				(2.84 - 20.82)	(112840 - 843171)	(7346 - 56316)
CPA [§]		Enderbury	0.65	8.36	197070	43602
				(2.9 - 20.9)	(95260 - 678828)	(14665 - 51030)
		Kanton	0.7	8.16	257718	41236
			(2.84 - 16.55)	(118094 - 789320)	(2534 - 52613)	
	PHO	McKean	0.6	7.09	621535	18881
			(2.98 - 15.25)	(158650 - 836223)	(4968 - 51387)	
			Niku	0.59	14.1	152035
				(3 - 30.55)	(66928 - 598129)	(9184 - 48625)
		Orona	0.48	7.7	269621	41680
				(2.93 - 15.31)	(137304 - 799518)	(4575 - 51152)
	PAL	Palmyra	0.73	13.39	142756	32542
				(4.16 - 27.22)	(62402 - 445380)	(9502 - 37524)
	POL	Fakarava	0.72	10.2	256744	40502
				(2.68 - 15.34)	(110875 - 780150)	(3091 - 49533)
Priors				* U [0.0001 ; 100]	U [100 ; 1500000]	U [100 ; 100000]

* The prior distribution of Nm is the product of two uniforms (one for N and one for m)

§ COR and CPA regions are from the Pacific Ocean (PAC).

Figure Legends

Figure 1. Map of the sampling sites. From west to east, Indian Ocean (IND): Juan (n = 13) and Zelee (n = 6); Chesterfield islands (CHE): Bampton (n = 10) and Avond (n = 5), New Caledonia (NCA): Belep (n = 7) and Poindimie (n = 5); Phoenix islands (PHO): Niku (n = 21), Mckean (n = 7), Orona (n = 11), Kanton (n = 10), Birnie (n = 2) and Enderbury (n = 13); Palmyra (PAL, n = 38); French Polynesia (POL): Moorea (n = 5), Fakarava (n = 17), Faaite (n = 1), Raraka (n = 1), and Nengo (n = 1). Colours represent the region of origin of the sampling sites: Indian Ocean (IND, yellow), Coral Sea (COR, red) and Central Pacific Ocean (CPA, blue).

Figure 2. Demographic scenarios investigated in all populations with $N_{ind} \geq 7$ through an Approximate Bayesian Computation (ABC) framework. N_{anc} : ancestral effective population size; T_c : time of effective population size change (NS only); N_{mod} : modern effective population size (NS only); T_{col} : colonization time of the array of demes (FIM and SST); D_{1-100} : demes (FIM and SST). Arrows represent the migrants exchanged (Nm) between demes. Details on each scenario are presented in the main text.

Figure 3. Correlation map between genetic diversity (θ_π) and Least Cost (LC) distances when considering Pacific Ocean sampling sites only. Each cell is coloured according to the correlation coefficient value computed between θ_π and the LC distance from the putative origin of the range expansion (RE). Black dots represent the sampling sites considered.

Figure 4. Variation of the effective population size (N_e) through time and its 75% confidence interval estimated by the *stairwayplot* for sampling sites of $n \geq 7$ in IND (a), COR (b) and CPA (c) regions.

Figure 5. Individual-based population structure analyses. Ancestry proportions retrieved using the *sNMF* algorithm with $K=2$ and $K=3$ ancestral populations (a) and Principal Component Analysis (b).

Figure 6. Population-based population structure analyses computed with populations of $n \geq 5$. Heat map representing the pairwise F_{ST} values between sampling sites (a) and Isolation by distance (IBD) plot considering Pacific sampling sites only (b).

Figures

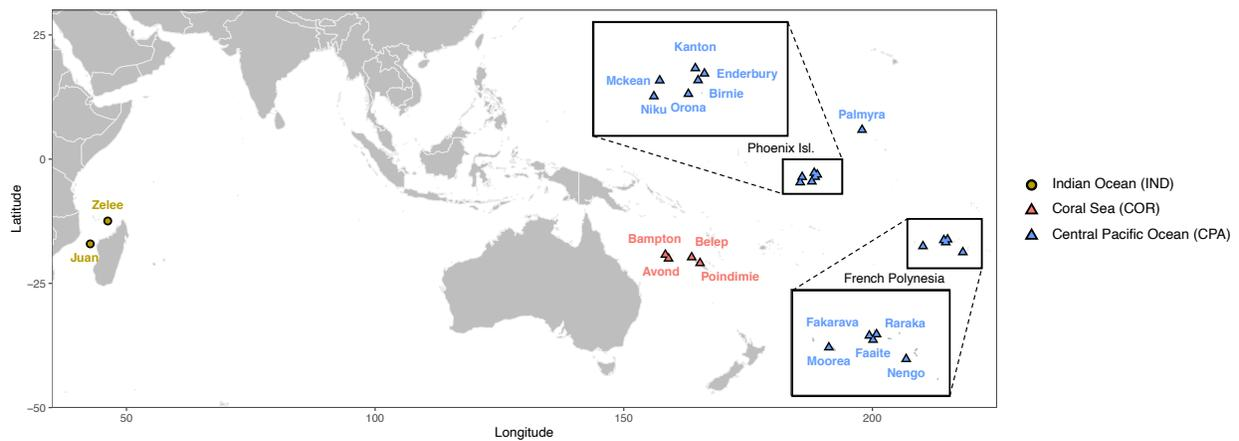


Figure 1. Map of the sampling sites. From west to east, Indian Ocean (IND): Juan ($n = 13$) and Zelee ($n = 6$); Chesterfield islands (CHE): Bampton ($n = 10$) and Avond ($n = 5$), New Caledonia (NCA): Belep ($n = 7$) and Poindimie ($n = 5$); Phoenix islands (PHO): Niku ($n = 21$), Mckean ($n = 7$), Orona ($n = 11$), Kanton ($n = 10$), Birnie ($n = 2$) and Enderbury ($n = 13$); Palmyra (PAL, $n = 38$); French Polynesia (POL): Moorea ($n = 5$), Fakarava ($n = 17$), Faaita ($n = 1$), Raraka ($n = 1$), and Nengo ($n = 1$). Colours represent the region of origin of the sampling sites: Indian Ocean (IND, yellow), Coral Sea (COR, red) and Central Pacific Ocean (CPA, blue).

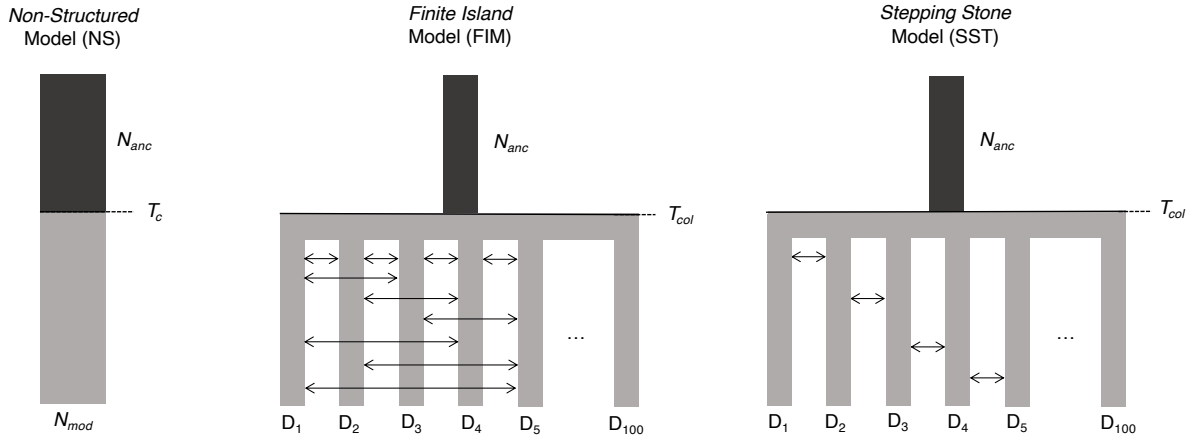


Figure 2. Demographic scenarios investigated in all populations with $N_{ind} \geq 7$ through an Approximate Bayesian Computation (ABC) framework. N_{anc} : ancestral effective population size; T_c : time of effective population size change (NS only); N_{mod} : modern effective population size (NS only); T_{col} : colonization time of the array of demes (FIM and SST); D_{1-100} : demes (FIM and SST). Arrows represent the migrants exchanged (Nm) between demes. Details on each scenario are presented in the main text.

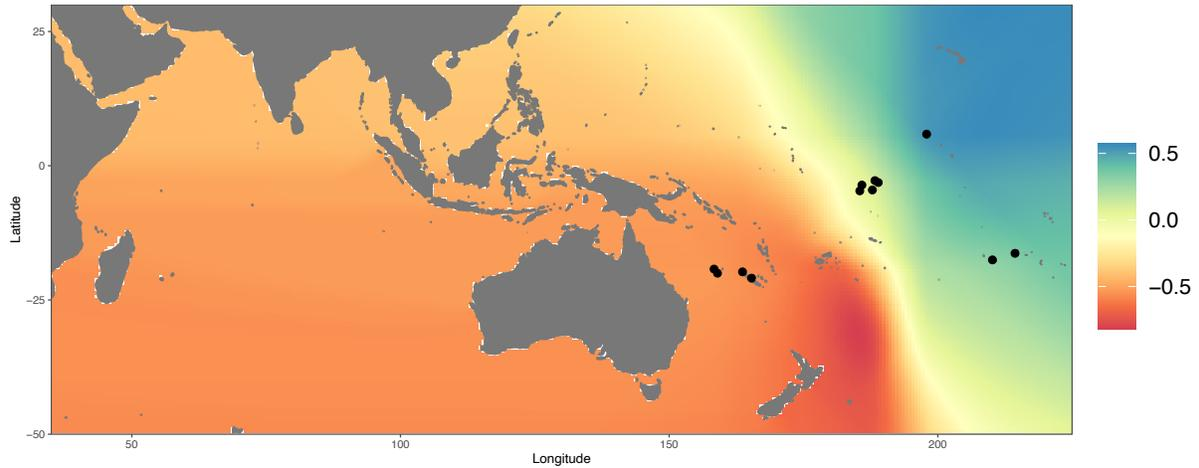


Figure 3. Correlation map between genetic diversity (θ_π) and Least Cost (LC) distances when considering Pacific Ocean sampling sites only. Each cell is coloured according to the correlation coefficient value computed between θ_π and the LC distance from the putative origin of the range expansion (RE). Black dots represent the sampling sites considered.

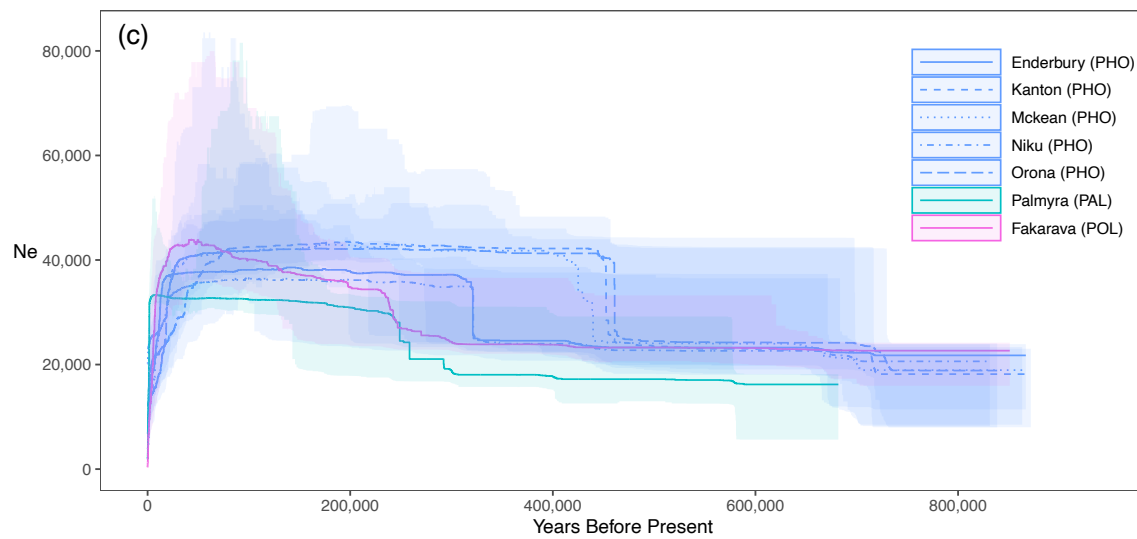
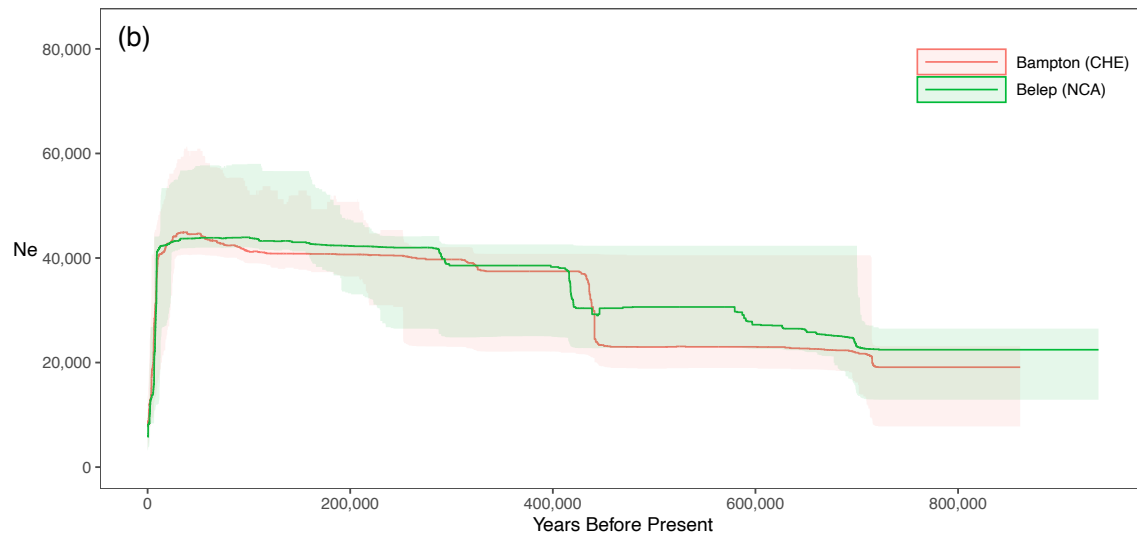
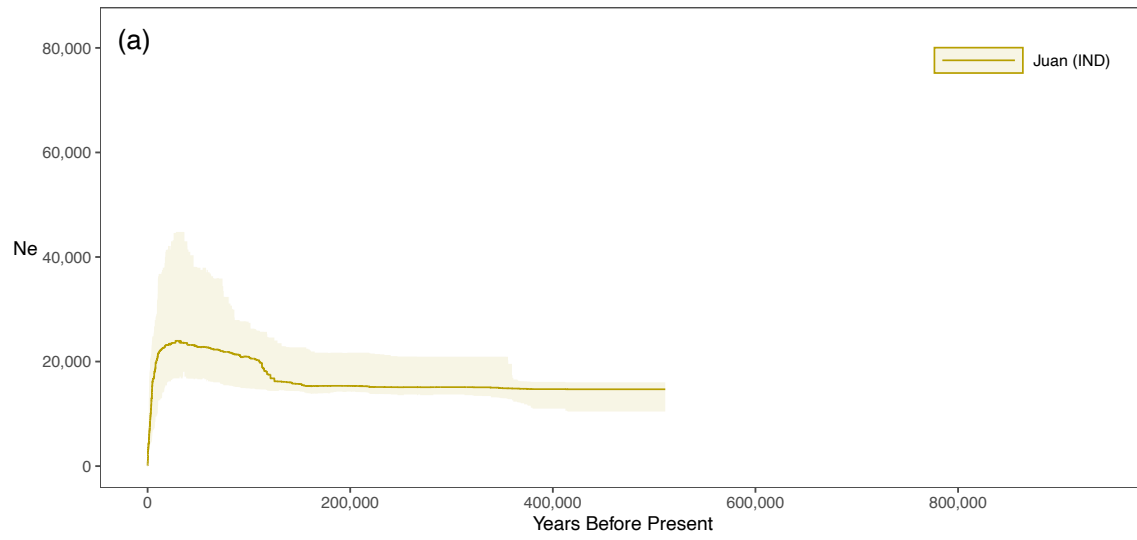


Figure 4. Variation of the effective population size (N_e) through time and its 75% confidence interval estimated by the *stairwayplot* for sampling sites of $n \geq 7$ in IND (a), COR (b) and CPA (c) regions.

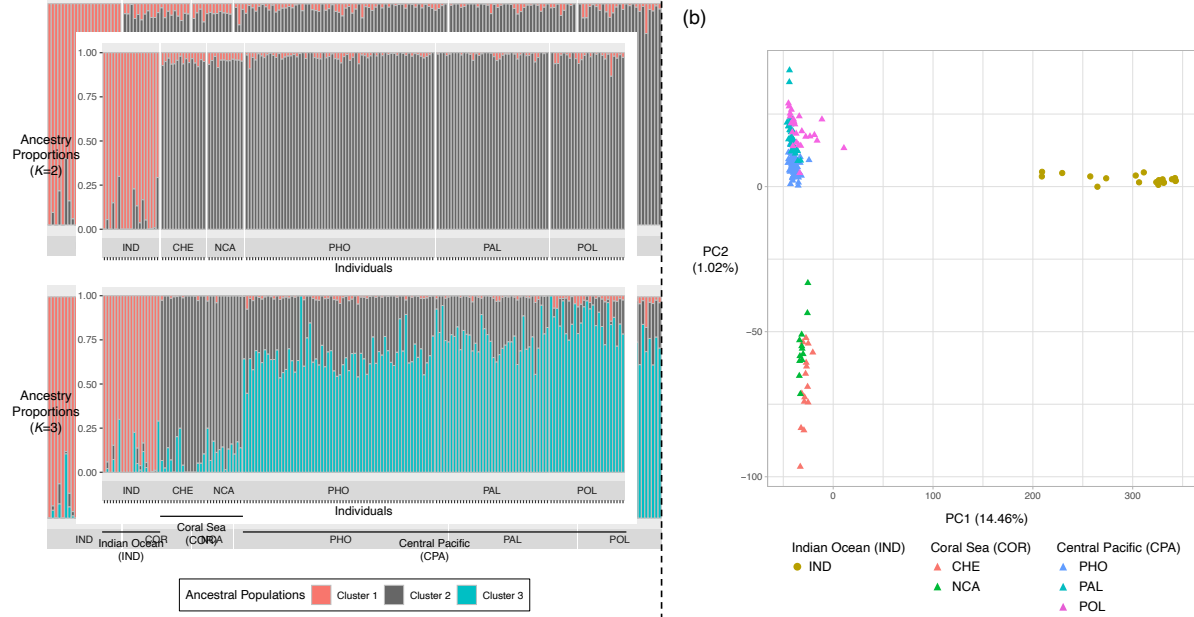


Figure 5. Individual-based population structure analyses. Ancestry proportions retrieved using the *sNMF* algorithm with $K=2$ and $K=3$ ancestral populations (a) and Principal Component Analysis (b).

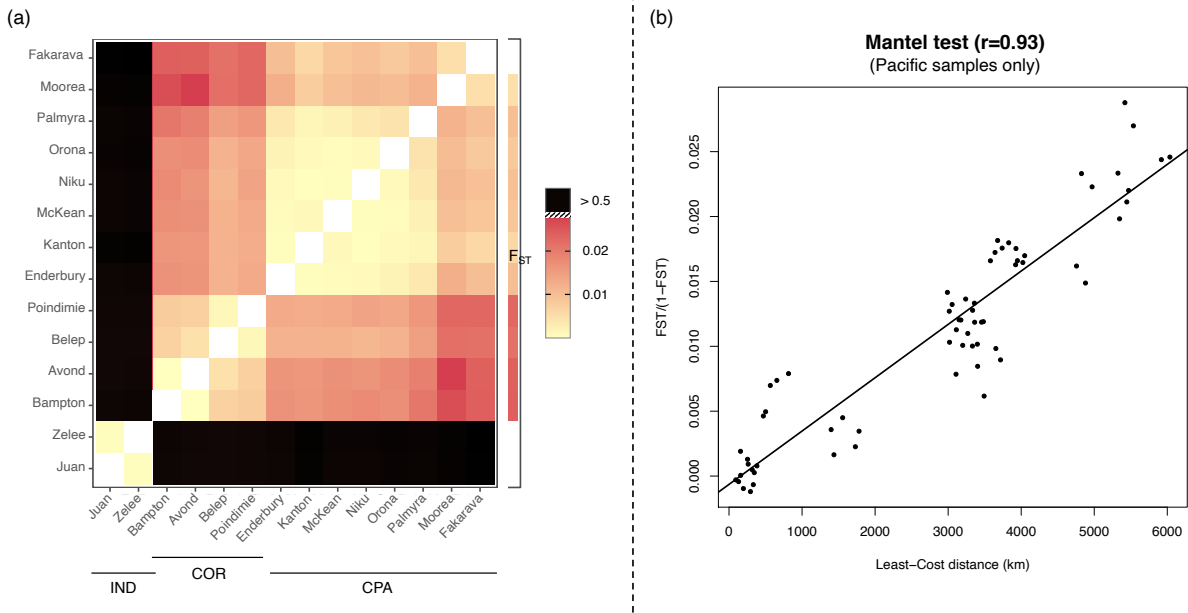


Figure 6. Population-based population structure analyses computed with populations of $n \geq 5$. Heat map representing the pairwise F_{ST} values between sampling sites (a) and Isolation by distance (IBD) plot considering Pacific sampling sites only (b).